Embedded atom simulations of titanium systems with grain boundaries

T. Hammerschmidt,[1,*] A. Kersch,[2] and P. Vogl[1]
[1]*Physik-Department and Walter Schottky Institute, Technical University Munich, Garching, Germany*
[2]*Infineon Technologies AG, Memory Products, Munich, Germany*
(Received 13 September 2004; revised manuscript received 5 January 2005; published 25 May 2005)

The atomistic simulation of polycrystalline growth with an empirical potential requires an accurate modeling of the atomic configurations at grain boundaries. We refine an existing embedded-atom potential for bulk titanium to reproduce systems with small atomic coordination, namely, clusters of up to nine atoms, the relaxation of the (0001) surface and the adatom diffusion on this surface. We find that simulating Ti growth can be limited to the (0001) surface and the rather small class of grain boundaries with angles of coincidence-site lattices. We determine the atomic structure of the Ti(0001) $\Sigma=7$ grain boundary with molecular statics and find exclusively pentagonal elementary structural units. The potential energy surface shows that this grain boundary imposes a massive barrier on surface diffusion. We use the elementary cells of the coincidence-site lattice to construct two periodic systems with grain boundaries: an isolated grain within an environment of different crystalline orientation and two antiparallel grain boundaries. Molecular dynamic simulations show that this isolated grain is not stable and that the growth evolution of the system with two antiparallel grain boundaries depends strongly on the angle of incidence.

DOI: 10.1103/PhysRevB.71.205409 PACS number(s): 61.72.Mm, 34.20.Cf, 81.15.Aa, 68.55.Jk

I. INTRODUCTION

Computational methods for predicting the growth of microstructures are of growing importance in materials research. The precise fabrication of nanoscale silicon structures calls for a profound understanding of the growth processes not only in the semiconductor layers but particularly in the metallization layers the present paper focuses on. Indeed, molecular dynamics and kinetic Monte Carlo methods[1–3] are widely used to simulate the growth mechanisms of materials (e.g., Al[4]). The predictive power of such simulations depends critically on the quality of the underlying many-body potentials. A well established method that has been shown to accurately reproduce a wide range of properties of metals is the embedded atom model.[5,6] In contemporary Si technology, thin films of Ti and TiN are used as diffusion stoppers between the semiconductor and aluminum contact layers.[8] The morphology of thin metallic films obtained by physical vapor deposition (PVD) depends strongly on the ratio of substrate temperature T_s to melting temperature T_m and ranges from single crystalline to granular.[9] Furthermore, this temperature ratio determines the minimum and maximum grain size. For Ti films, one has specifically $T_s=500$ K and $T_m=1600$ K which leads to grain sizes of 0.01 to 0.3 μm.[10–12] These sizes are comparable to or smaller than the surface diffusion length, in contrast to materials such as Al, where grain sizes are much larger and therefore play little role in the growth process. Consequently, an accurate simulation of Ti thin-film growth requires a proper inclusion of finite grains. This imposes several difficulties for a simulation: neither does one know the boundary conditions nor the atomic positions *a priori*. In addition, realistic molecular dynamics calculations of grain boundaries and surfaces require a many-body potential that is adopted to the low atomic coordination in such situations. For Ti, an accurate embedded atom potential has been determined before,[13] albeit only for bulk Ti and not for clusters, surfaces, or interfaces with low coordination numbers.

In this work, we have determined an accurate embedded-atom potential that maintains the bulk properties of the potential of Ref. 13, including its improvements by Ref. 14, but additionally captures the known bond lengths and binding energies of small Ti clusters (containing 2–9 atoms) and several properties of the Ti(0001) surface accurately. With this potential, we have determined the atomic structure and the elementary structural units of the relaxed $\Sigma=7$ (0001) coincidence-site lattice (CSL) grain boundary and calculated the binding energies of adatoms near the grain boundary, as well as the diffusion barriers within and across the grain boundary. We have performed extensive molecular dynamics studies of isolated Ti grains embedded in a crystalline environment of different lateral orientations and predict the stability of grains as a function of their size and of temperature. In addition, the effect of atomic deposition on the surface morphology near grain boundaries is investigated. Generally, only few publications have addressed polycrystalline growth so far. One type of approach is based on the kinetic Monte Carlo method that operates on a crystalline lattice but introduces an arbitrary index to represent individual grain orientations.[4] More realistic but very demanding computational schemes allow arbitrary atomic positions (termed off-lattice kinetic

TABLE I. Parameters for the atomic density $\rho(r)$.

r_i [Å]	a_i [$1/Å^3$]
5.09113442[a]	0.5476138534[a]
4.38171405[a]	−0.5512656007[a]
2.7[b]	40.0[b]
2.5[b]	−25.0[b]

[a]Ref. 13.
[b]This work.

TABLE II. Parameters for the pairwise interaction $\phi(r)$.

r_i [Å]	a_i [eV/Å^3]
5.09113442[a]	−0.7857149938[a]
5.00767320[a]	1.110966254[a]
4.67382832[a]	−0.2994497740[a]
3.96440795[a]	−0.1430612718[a]
3.33844880[a]	1.025367788[a]
2.950800645[a]	0.4942930559[a]
2.9[b]	6.0[b]
2.7[b]	−3.41[b]

[a]Ref. 13.
[b]This work.

Monte Carlo methods) and recalculate the possible atomic diffusion paths in each time step. Presently, such methods are still limited to idealized potentials or rather small systems.[15,16]

In general, there is an infinite number of possible orientations of adjacent grains relative to each other. In the case of Ti the number of relevant grain boundary arrangements can be significantly reduced by focusing on PVD growth. Experimental data show hexagonal close packed structures dominated by growth in the hexagonal [0001] direction.[11,17,18] Furthermore, the energetically most favorable[19] grain-boundary angles are known to be values that form so-called coincidence-site lattices.[20–22] These are lattices that are formed by the common atomic positions of two intersecting rotated crystalline lattices.[23,24] In Ti thin films, the experimentally observed angles of $\varphi_{\mathrm{CSL}}=21.8°$,[22] 12.29°,[25] and 69.43° (Ref. 26) agree perfectly with coincidence-site angles. Indeed, some of the underlying atomic structures resemble symmetric coincidence-site lattices [e.g., $\varphi_{\mathrm{CSL}}=21.8°$ (Refs. 27 and 28)], whereas others indicate rather complex dislocation networks.[25,29]

These findings allow us to assume in this paper that many morphological effects of thin-film growth of Ti can be captured by focusing on [0001] oriented grains that are laterally rotated by certain CSL angles with respect to each other. In Sec. II, we define the Ti embedded-atom potential and determine its parameters. In the following Sec. III, we discuss the microscopic geometry of the $\Sigma=7$ grain boundary and determine the binding energy of an adatom near this grain boundary. In Sec. V, molecular dynamics simulations of an isolated grain and a pair of antiparallel grain boundaries are presented. The main results are summarized in Sec. VI.

II. POTENTIAL

In this section, we define the embedded-atom potential[5–7] model that we have optimized for various titanium properties. The embedded-atom method (EAM) treats the individual atoms as embedded within the electron density of the remaining system and is particularly suited for metallic systems with delocalized valence electron distributions.

TABLE III. Parameters for the cubic spline representation of the embedding function $F(\rho)$ for $0\leqslant\rho\leqslant48$. Note that the derivatives at the boundary values define the spline interpolation uniquely.

ρ [dim.less]	$F(\rho)$ [eV]	$F'(\rho)$ [eV/Å]	$F''(\rho)$ [eV/Å^2]
0.00	0.00	−0.3	$2.324535081465755\times10^{-2}$
10.00	−2.45		$-1.349070162931513\times10^{-2}$
20.00	−4.85		$3.371745570260303\times10^{-2}$
30.00	−5.45		$-1.337912118109709\times10^{-2}$
40.00	−6.30		$4.799029021785401\times10^{-3}$
48.00	$-\sqrt{48}$	$-(2\sqrt{48})^{-1}$	$-1.578195999192991\times10^{-5}$

A. Bulk embedded-atom potential

In the EAM, the atomic potential energy E_i of atom i located at $\mathbf{x}_i$ is given by the embedding energy $F(\rho_i)$ plus the repulsive two-body interaction $\phi(|\mathbf{x}_i-\mathbf{x}_j|)$ with its neighbors j

$$E_i = F(\rho_i) + \sum_{j(\neq i)} \phi(|\mathbf{x}_i - \mathbf{x}_j|). \tag{1}$$

The total potential energy of the system is taken as the sum over all E_i.[5–7] The dimensionless atomic density ρ_i at atom i is written as

$$\rho_i = \sum_{j(\neq i)} \rho(|\mathbf{x}_i - \mathbf{x}_j|). \tag{2}$$

In the previously published implementation of Ref. 13 for titanium, the embedding function has been chosen to be $F(\rho_i)=-\rho_i^{1/2}$ and the functions $\rho(r)$ and the pair interaction $\phi(r)$ have both been represented in the form

$$f(r) = \sum_{i=1}^{n} a_i (r_i - r)^3 \theta(r_i - r). \tag{3}$$

Here, $\theta(x)$ is the Heavyside function and $n=2$ for $\rho(r)$ and $n=6$ for $\phi(r)$, respectively. The parameters a_i and the radii r_i are listed in Tables I and II for later reference. They have been determined in Ref. 13 to reproduce bulk properties.

B. Reference data

For a proper simulation of grain boundaries, one needs to reproduce systems of low atomic coordination and of low atomic density, in addition to bulk systems. In this section, we summarize the experimental and theoretical reference data (see Table II) that we have used for determining and

TABLE IV. Comparison of properties of Ti clusters, as obtained previously, with results calculated in this work either with the published potential of Ref. 13 or with the potential developed in this paper. Here, l is the average bond length and E_b the binding energy in Ti clusters, Δ_{ij} the relative change in the distance between the top layers i,j of the Ti(0001) surface with respect to the bulk distance d_{vol}, γ the relaxed surface energy, and Q_i are the energy barriers for adatom diffusion on the specified surfaces. The precise meaning of Q_1 and Q_2 is explained in the main text.

	Ti clusters and surfaces			
	previous work		this work	
	theory	experiment	Ackland	new potential
$l(Ti_2)$ [Å]	1.94[a]	1.94[b]	2.55	2.00
$l(Ti_3)$ [Å]	2.35[a]		2.68	2.30
$l(Ti_4)$ [Å]	2.52[a]		2.75	2.63
$l(Ti_5)$ [Å]	2.51[a]		2.77	2.71
$l(Ti_6)$ [Å]	2.55[a]		2.78	2.75
$l(Ti_7)$ [Å]	2.63[a]		2.80	2.81
$l(Ti_8)$ [Å]	2.70[a]		2.79	2.82
$l(Ti_9)$ [Å]	2.59[a]		2.80	2.83
$E_b(Ti_2)$ [eV]	1.54[a]	1.54[c]	1.94	1.59
$E_b(Ti_3)$ [eV]	1.99[a]		2.53	1.94
$E_b(Ti_4)$ [eV]	2.57[a]		2.94	2.72
$E_b(Ti_5)$ [eV]	3.02[a]		3.14	3.21
$E_b(Ti_6)$ [eV]	3.35[a]		3.33	3.64
$E_b(Ti_7)$ [eV]	3.60[a]		3.42	3.69
$E_b(Ti_8)$ [eV]	3.62[a]		3.35	3.65
$E_b(Ti_9)$ [eV]	3.83[a]		3.51	3.81
$\Delta d_{12}/d_{\mathrm{vol}}$ (%)	−7.7[d]	−4.9[e]	−0.40	−1.7
$\Delta d_{23}/d_{\mathrm{vol}}$ (%)	+2.8[d]	+1.4[e]	+0.41	+0.25
$\gamma(0001)$ [meV/Å^2]	137[d]	102.99[f]	62.28	73.99
$\gamma(2\bar{1}\bar{1}0)$ [meV/Å^2]			74.12	63.67
$\gamma(01\bar{1}0)$ [meV/Å^2]			66.19	71.78
Q_1 (0001) [eV]		0.35–0.40[g]	0.17	0.38
Q_2 (0001) [eV]		0.35–0.40[g]	0.14	0.37
Q_1 $(2\bar{1}\bar{1}0)$ [eV]			0.71	1.06
Q_2 $(2\bar{1}\bar{1}0)$ [eV]			1.36	2.23
Q_1 $(01\bar{1}0)$ [eV]			0.26	0.57
Q_2 $(01\bar{1}0)$ [eV]			1.05	2.02

[a]Ref. 31.
[b]Ref. 30.
[c]Ref. 33.
[d]Ref. 36.
[e]Ref. 38.
[f]Ref. 46.
[g]This work.

setting up the present EAM potential.

The Ti dimer bond length[30–32] and its binding energy[31–34] have been extensively studied both experimentally and theoretically. For clusters with more than two atoms, there are only *ab initio* results available.[31,32] These theoretical results show the overbinding effect that is typical for local density functional calculations. Therefore, we have shifted these published binding energies by a constant to match the experimentally observed dimer binding energy. The relaxation of the Ti(0001) surface can be characterized by the two topmost layer distances and is well established.[35–38]

A surface related quantity that is less well known is the activation barrier for the Ti adatom diffusion on Ti surfaces. While there are no direct measurements of this quantity, there are extensive studies of Ti deposition on tungsten substrates.[39–41] It is well established that Ti forms a pseudomorphous (0001) surface on bcc W(110) substrates.[39,42] These experiments showed that the work function reaches a stable value of 3.5 to 4.0 eV after a few monolayers of Ti are deposited.[39,41] There is an empirical relation $Q \approx 0.1 E_b$ between the work function E_b and the activation barrier Q,[43] that works well for Ti adatoms on other tungsten surfaces.[39,44] We therefore used this procedure to estimate the activation barrier for surface diffusion of a Ti adatom on Ti(0001) to lie between 0.35 an 0.40 eV. This value is significantly larger than the previous result of 0.04 eV from a molecular dynamics simulation[45] with the potential of Ref. 13.

C. Development and validity of new potential

The Ti properties for low coordination numbers depend critically on the EAM potential for radii r smaller than the lattice constant and for atomic densities ρ_i lower than the crystalline density. We have therefore developed a new EAM potential that uses the form given in Eq. (1), but with an embedding function that is represented in terms of a cubic spline for small atomic densities and is given by $F=-\rho^{1/2}$ only in the limit of large densities. Concretely, we have used this asymptotic expression for $\rho > 48$ in view of the fact that the hcp bulk density corresponds to a value of $\rho = 48.84$. In addition, both the atomic density $\rho(r)$ and the two-body repulsion term $\phi(r)$ of the form of Eq. (3) have been extended so that four terms ($n=4$) are included in $\rho(r)$ and eight terms ($n=8$) contribute to $\phi(r)$, respectively. The parameters for the presently developed potential are given in Tables I–III. We note that the first two and six lines in Tables I and II, respectively, are identical to the previously determined potential values.[13] This guarantees that the present potential reproduces the established bulk Ti properties.

In Table IV, we compare previously calculated and experimentally measured properties of Ti with the results obtained by the present model. The top section shows average values for the bond lengths $l(\mathrm{Ti}_{\mathrm{cluster}})$ and binding energies $E_b(\mathrm{Ti}_{\mathrm{cluster}})$ of several relaxed clusters. The middle part displays the calculated and measured (0001) surface relaxations. To be precise, we list the change in distance between the first and second top layer Δd_{12} and between the second and third top layer Δd_{23}, respectively, relative to the interlayer bulk distance d_{vol}. Finally, the table shows the surface energies γ and the diffusion barriers for various Ti surfaces. For the (0001) surface, there are two inequivalent stable adatom positions, namely, the hcp and fcc position. For the other surfaces, there is only one stable position but the adatoms may diffuse along an atomic row or perpendicular to it. For all these cases, the corresponding diffusion barriers are denoted by Q_1 and Q_2, respectively. The second and third columns in Table IV show previously published results whereas the fifth column gives the results obtained by the present potential. For comparison, we have also calculated all of these quantities in terms of the original bulk potential of Ref. 13. The latter results are given in the fourth column. As one can see generally, the present potential accurately predicts the established cluster results as well as the surface properties of Ti.

The predicted average bond lengths and binding energies of the clusters differ by less than 10% from the *ab initio* and experimental results. The activation barrier for surface diffusion that plays an important role for epitaxial growth, is also very well reproduced. The relaxation of the two outermost atomic layers of the (0001) surface and the energy of the relaxed (0001) surface are only slightly improved compared to the results obtained with the potential of Ref. 13. This is probably due to the anisotropic bonding character near the surface that is not incorporated in any EAM potential. Finally, we have repeated the calculation of the extrinsic stacking fault *ABABCABAB* on the basal plane that has been studied in great detail together with other stacking faults in Ref. 13. Since a stacking fault is predominantly a bulk property, our potential yields virtually the same results: the stacking fault energies on the basal plane are underestimated as compared to experiment.[47]

Several previous theoretical studies of screw dislocations and slip systems in titanium[48–51] have revealed that stacking fault energies as well as surface energies are sensitive to the formation of directed covalent-type bonds which are missed in isotropic potential schemes such as the present EAM method. However, it was also found that the structural and mechanical stability of titanium with respect to large deformations is well reproduced by the EAM scheme.[50,51] The present potential can be extended to describe high-energy collisions by introducing additional short-range terms.[52]

D. Numerical details

The initial geometries of the clusters have been taken from previous *ab initio* results[31] and relaxed until the absolute magnitude of the maximum force F_{max} on each atom was lower than 10^{-6} eV/Å. The resulting clusters have higher symmetry than obtained by *ab initio* calculations which stems from the isotropic character of the EAM potential. The relaxation of the two outermost atomic layers of the Ti(0001) surface was calculated with a slab consisting of eight atomic layers. The two equilibrium distances d_{12} and d_{23} between the three outermost layers were determined by minimizing the total energy with respect to d_{12} and d_{23} simultaneously. The activation barrier for diffusion on the calculated Ti surfaces was taken to be the difference between the binding energy of an adatom in a stable position and at the point of minimum binding energy on the straight path between two stable positions. In the calculation of the binding energy for a given adatom position (x,y) at a height h above the surface, we have relaxed all substrate atoms that lie within twice the cutoff radius of the potential until $|F_{\mathrm{max}}| < 10^{-6}$ eV/Å was reached. This procedure was repeated for several values of the height h until the total energy as a function of h became minimal.

III. STRUCTURE OF GRAIN BOUNDARY

We have used this accurate EAM potential to investigate systems with a given coincidence site lattice (CSL) grain

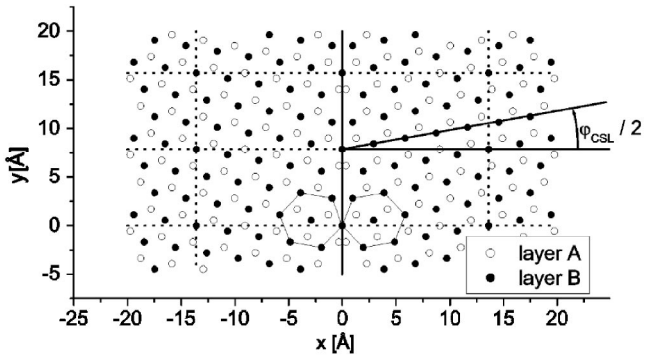

FIG. 1. The symmetric Ti(0001) CSL grain boundary corresponding to $\Sigma=7$ ($\varphi_{CSL}=21.79°$). The superlattice cells of the corresponding periodic coincidence-site lattice are indicated by dotted lines. The thin lines marking the hexagons on both sides of the interface are drawn to guide the eye.

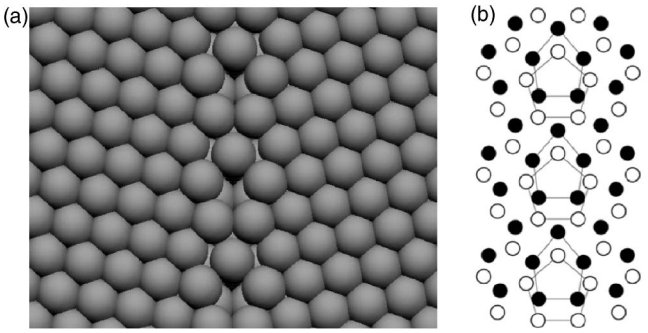

FIG. 2. The symmetric $\Sigma=7$ Ti(0001) CSL grain boundary (Fig. 1) after relaxation. (a) The surface layer shows a small region of reconstruction and pentagonal structural elements. (b) In lower-lying layers we find also exclusively pentagonal elements in contrast to previous works (Refs. 27, 28, and 53). The elements of the surface layer differ from those of a similar layer in an infinite system by 0.118–0.169 Å.

boundary. In this section, we analyze the atomistic structure near this grain boundary, the Ti adatom surface diffusion near and across it, as well as the epitaxial growth on top of this grain boundary.

A. Ideal grain boundary

Ti films that are grown with PVD are dominated by the (0001) facet and CSL grain boundaries (Sec. I). Consider two identical hcp crystal lattices $\mathcal{A}$ and $\mathcal{B}$ that are rotated with respect to each other about the common [0001] axis. For certain azimuthal rotation angles, these two lattices share a set of common lattice sites from *A* and *B*. These common sites form a periodic superlattice that is called coincidence-site lattice.[23] The quotient of the number of atomic sites within the CSL superlattice cell and within the hcp crystal unit cell is termed coincidence ratio Σ. Since an hcp lattice contains two atoms per hexagonal unit cell, the number of atoms within a CSL superlattice cell is $2\times\Sigma$. An ideal CSL grain boundary can be formed as follows. For a given value of Σ, we consider superlattice cells that consist solely of atomic sites of lattice $\mathcal{A}$ and superlattice cells with atomic sites of lattice $\mathcal{B}$. An ideal symmetric CSL grain boundary can now be formed by putting these two types of superlattices adjacent to each other. In Fig. 1, we show such an ideal symmetric CSL grain boundary for the rotation angle $\varphi_{CSL}=21.79°$ which corresponds to $\Sigma=7$. The figure depicts the atoms (full and empty circles, respectively) in two vertically adjacent hcp layers. The supercells are marked by dotted lines.

These ideal grain boundaries are mathematical constructs that lead to configurations where atoms may lie too close to each other. In order to determine the real atomic structure near a grain boundary, one therefore needs to minimize the total energy of a system and compare the energies per atom for many configurations where some of the ideal positions are initially left empty. Therefore, the ideal grain boundary configuration shown in Fig. 1 only serves as a starting point for such a calculation.

B. Real grain boundary

The initial geometry of the CSL grain boundary shown in Fig. 1 was set up as a slab with twenty atomic layers in [0001] direction. The interface was formed by three superlattice cells on each side (see Fig. 1) of the interface and periodic boundary conditions in the (0001) plane were imposed. We fixed the atomic positions in their ideal crystal position for atoms more than 10 Å away from the interface and allowed for arbitrary relaxation of the atoms within that distance. This distance of 10 Å is twice the typical width of a grain boundary[19] and was sufficient to reduce the maximum force on any interface atom to a value below 10^{-6} eV/Å. We considered several grain boundaries with different numbers of atoms in the interface region, consequently relaxed their positions, and calculated the average potential energy per atom. In this optimization process, we additionally rejected final configurations that contained morphological defects, i.e., formed holes or led to an accumulation of atoms at the surface of the slab. The former and the latter configurations are caused by too few and too many atoms in the interface region, respectively. The final relaxed structure with the minimum average binding energy is shown in Fig. 2(a). Importantly, we find the atomic configurations at the grain boundary in all layers to consist of pentagons. We find this result to be independent of the chosen initial configuration. This result is somewhat at variance with previous publications that employed purely bulk-optimized empirical potentials.[27,28,53] These authors found structural units consisting of alternating pentagonal and tetragonal symmetry in adjacent (0001) layers. We note that we obtain pentagonal structural elements in all layers already with the original bulk potential.[13]

In order to investigate the influence of the surface onto the grain boundary, we repeated the calculations by imposing periodic boundary conditions in the [0001] direction. It turned out that the interface in an infinitely extended system contains the same pentagonal elements as the slab with two relaxed surfaces [as shown in Fig. 2(b)]. Only the atomic positions differ by values of the order of 0.1 Å.

We have also repeated the slab calculations with another EAM potential where we have redetermined its parameters so that the binding energies of the clusters agree with the original LDA values[31] rather than with the shifted ones given

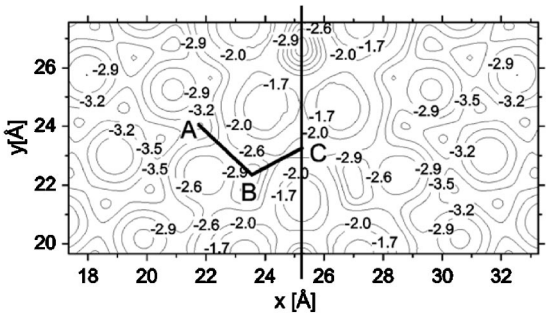

FIG. 3. Contour graph of the binding energy of a Ti adatom in the neighborhood of the relaxed $\Sigma=7$ Ti(0001) CSL grain boundary, in eV. Here, A, B, and C are stable adatom positions near the grain boundary and the diffusion paths between them are indicated by thick lines. The thin line marks the grain boundary.

in Table IV. The remaining physical properties remained the same. Interestingly, this potential does not lead to a stable symmetric grain boundary, in contrast to what is observed experimentally. This supports the accuracy of the present potential.

IV. DIFFUSION NEAR GRAIN BOUNDARY

We have investigated the influence of the grain boundary on the surface diffusion of an adatom by calculating its binding energy in various lateral positions near the grain boundary. The computational procedure corresponds to the determination of the diffusion barrier on the (0001) surface as described in Sec. II D. The resulting potential energy surface in the surrounding of the grain boundary is shown in Fig. 3. The energy barriers for transitions from the position A to B and from B to C near the interface amount to $\Delta E_{AB}=1.11$ eV and $\Delta E_{BC}=1.21$ eV, respectively. These values are significantly higher than the barrier for diffusion on an ideal Ti(0001) facet which we find to be $\Delta E_{(0001)}=0.38$ eV. Thus, the grain boundary is a massive barrier for surface diffusion of adatoms.

This can be seen more clearly in Fig. 4 which shows the adatom binding energy along the diffusion path from the hcp to the fcc surface position on an ideal (0001) surface as well as along the trajectories $A\rightarrow B$ and $B\rightarrow C$, respectively. The activation energy increases from 0.38 eV on an ideal (0001) surface to 1.11 eV for diffusion along the grain boundary and 1.21 eV across it. As can be deduced from Fig. 3, the influence of the grain boundary vanishes more than 5 Å away from the interface. This is in accord with the observed width of about 10 Å of structural changes induced by a grain boundary.[19]

V. GROWTH ON TO GRAIN BOUNDARY

The realistic prediction of epitaxial growth of Ti requires an understanding of the influence of grains on the growth mechanisms. Important questions include the size and stability of grains, the type of epitaxial growth on top of and near grain boundaries and the structural relaxations induced by grain boundaries.

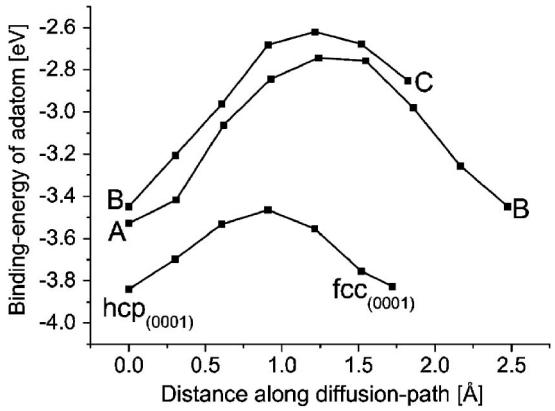

FIG. 4. Binding energy of a Ti adatom near the Ti(0001) $\Sigma=7$ grain boundary along several trajectories. The positions A, B, and C correspond to those shown in the previous figure. The two stable adatom positions on an ideal (0001) surface are denoted by hcp and fcc, respectively.

A. Stability of isolated grains

An isolated grain consists of a small region of crystalline orientation $\mathcal{A}$ enclosed by an environment of a different orientation $\mathcal{B}$. We have simulated grains of various shapes and sizes, and investigated systematically their stability with respect to temperature and grain size.

First, we have investigated the stability of very small grains. In particular, we have considered a grain that is formed by a block of 6 CSL cells (Fig. 1) of orientation $\mathcal{A}$ surrounded by eight similar blocks of orientation $\mathcal{B}$. This isolated grain has dimensions of 13.56 by 7.83 Å. A slab geometry consisting of 20 layers and periodic boundary conditions in the (0001) plane has been used, similar to what has been described in Sec. III B. The two surfaces of the slab are sufficiently far apart that they do not influence each other. Subsequently, we have relaxed all atoms that lie in a distance of less than 10 Å from the interface area until $|F_{\max}|<10^{-6}$ eV/Å. In effect, this amounts to keeping both the core of the grain as well as the outer surrounding at fixed misorientation relative to each other. In other words, the grain cannot decay in this simulation but it can change its shape. The number of atoms has been varied until a low energy and defect-free grain boundary is formed as discussed in Sec. III B. As a result, we find the relaxation to alter the originally rectangular shape of the isolated grain into a circular shape with a diameter of about nine lattice constants. The upper ten layers of the final relaxed slab are shown in Fig. 5.

Second, we studied the stability of this system by relaxing the geometrical constraints and tempering the system. To be precise, we froze the atomic grain configuration just discussed in the central six layers of the slab and allowed all atoms in the remaining layers to relax freely. In addition, we set the temperature to 300 K by performing molecular dynamics calculations with the thermostat of Berendsen.[54]

Snapshots of the initial configuration and another one after 20 ps are shown in Fig. 6. This figure shows cross sections of the seven layers above the fixed central layers in the plane perpendicular to the [1000] direction. This direction

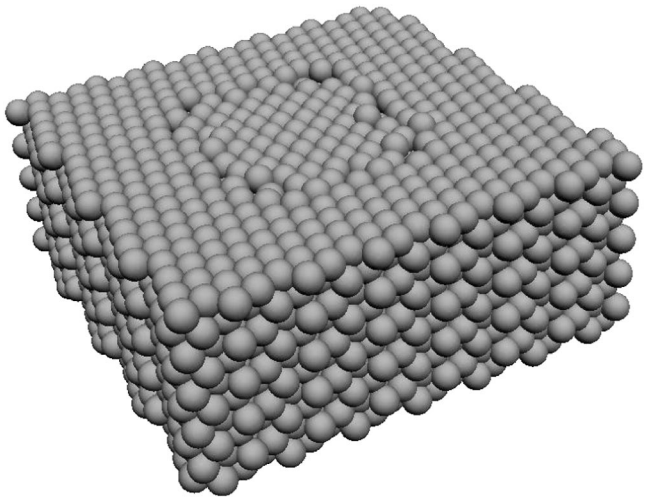

FIG. 5. A slab of twenty layers with an isolated grain. The atoms in less than 5 Å distance from the boundary planes have been fully relaxed.

corresponds to the orientation of the outer region of the simulated area. Their atoms appear as regular point lattice. The misorientation of the atoms in the central region, on the other hand, appears as a quasicontinuum of atomic positions in this projection. The snapshots of Fig. 6 show that the isolated grain decays rapidly in the sense that it changes its crystalline orientation to match the one of its surrounding. This reorientation causes an incomplete atomic filling of the surface layer which therefore contains point defects. This deviation from crystallinity is clearly visible in Fig. 6. The layers beneath become filled and therefore form a regular lattice.

As one might expect, the stability of an isolated grain depends on its size and on the system temperature. We have performed simulations of the same small grain as above, consisting of six CSL cells (Fig. 1), but at lower temperatures of 250, 200, and 150 K. In the former two cases, we also find a decay of the grain, but the decay time is increased to 50 ps and 100 ps, respectively. At 150 K, no significant structural changes of the isolated grain were observed up to 1 ns.

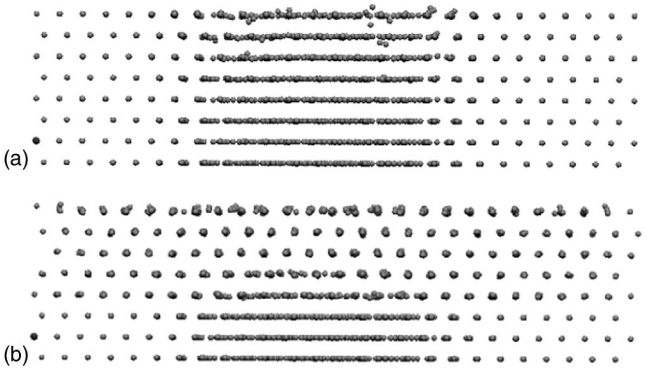

FIG. 6. The atomic positions of the isolated grain from Fig. 5, viewed along the [1000] direction in the initial relaxed configuration (a) and after a molecular-dynamic simulation of 20 ps at 300 K (b). The isolated grain is seen to decay. The lower three layers were kept fixed in the simulation.

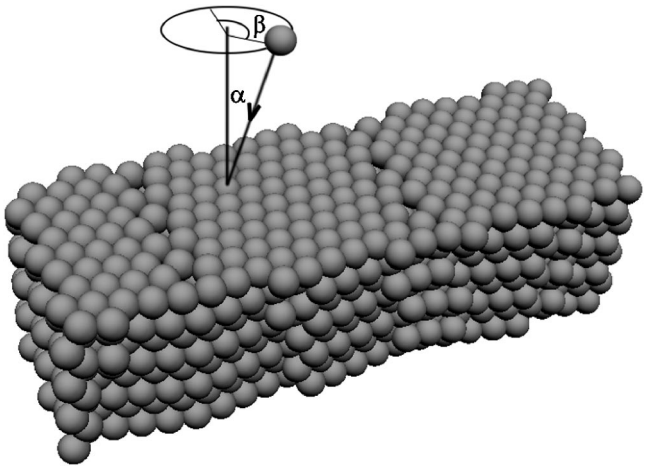

FIG. 7. Two relaxed antiparallel grain boundaries in the (0001) plane. We investigated deposition with $\alpha=20°$ and either $\beta=0°$ or $\beta=90°$.

The size dependence of the grain stability was investigated by taking larger grains consisting of 12 and 24 CSL cells (Fig. 1), corresponding to diameters of 33 and 44 Å, respectively. At room temperature, these systems maintained their misorientation and appeared to remain stable for at least several hundred ps (the maximal simulation time). This result is indeed plausible and corresponds to the well known island formation of adatoms on surfaces which also requires a minimum size of atomic conglomerates. In the present case of Ti, we find the minimum diameter of a stable isolated grain to be of the order of 33 Å. This value is comparable to the minimum grain size of 100 Å that was found experimentally so far.[10]

B. Growth on a grain boundary

We have investigated homoepitaxial growth of Ti onto a surface that contains a tilt grain boundary, focusing on questions of crystallinity and its dependence on growth conditions such as the angle of incidence of Ti atoms. A system with a single tilt grain boundary has the lateral structure $\mathcal{A}:\mathcal{B}$, where $\mathcal{A}$ and $\mathcal{B}$ are CSL cells of a given crystalline orientation as explained before. Obviously, such a system is not periodic. Its simulation would therefore require us to use fixed boundary conditions that would influence the result in an uncontrollable fashion. We have therefore set up periodic supercells of type $(\mathcal{A}:\mathcal{B})_\infty$, $(\mathcal{A}:\mathcal{B}:\mathcal{A})_\infty$, or $(\mathcal{A}:\mathcal{B}:\mathcal{B}:\mathcal{A}:\mathcal{A})_\infty$ that contain two grain boundaries, albeit in a sufficiently large distance from each other so that no noticeable interaction influences the results (see Fig. 7). The investigation of supercells that are larger than the minimum periodicity cell $\mathcal{A}:\mathcal{B}$ is motivated by the fact that a tilt grain boundary may cause longer range correlations that can only be seen in larger periodicity cells. For the same reason, we included two CSL cells also in the direction parallel to the grain boundary (giving a maximum of ten CSL cells in one plane of the simulation cell).

We performed a series of molecular-dynamics simulation of slabs containing two antiparallel grain-boundaries. There

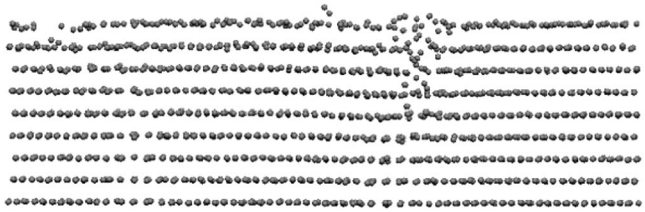

FIG. 8. The antiparallel grain boundaries (Fig. 7) after deposition of five atomic layers within 250 ns at $T=300$ K. Deposition exclusively perpendicular to the boundary planes ($\beta=90°$) shows layer-by-layer growth and the appearance of amorphous regions.

FIG. 9. The antiparallel grain boundaries (Fig. 7) after deposition of five atomic layers within 250 ns at $T=300$ K. The same simulation as in Fig. 8 with deposition exclusively parallel to the boundary planes ($\beta=0°$) shows similar layer-by-layer growth, but significantly bigger amorphous regions.

are 20 atomic layers in the [0001] direction (and therefore two surfaces) and periodic boundary conditions in both lateral directions, containing about 1650 atoms. An initial atomic configuration of the slab system was determined by relaxing the position of all atoms with less than 10 Å distance from the boundary planes (see Sec. III B). Based on this configuration, we have subsequently analyzed epitaxial growth onto this structure. To this end, we used only the upper half of the slab (and therefore only one surface) as shown in Fig. 7. First, we fixed the temperature at 300 K (Ref. 54) and kept the atomic positions of the atoms in the lower three layers fixed but allowed the remaining atoms to move freely. We have verified that this structure is thermally stable.

In the following step, we have deposited atoms with an initial kinetic energy of E_{kin} and with impinging angles characterized by two angles α and β. The angle α is the angle between the initial trajectory and the surface normal, whereas β is the azimuthal angle relative to the grain interface. The lateral positions of the impinging atoms were chosen randomly, their initial height above the surface exceeded the cutoff radius of the potential. We have focused our studies on incident angles and kinetic energies where we expect large sticking coefficients, namely, $\alpha=20°$ and $E_{\mathrm{kin}}=20$ eV.[14] In this way, 1000 atoms or approximately five atomic layers have been deposited at a fixed temperature of 300 K. In Figs. 8 and 9, we show results for deposition parallel to ($\beta=0°$) and perpendicular to ($\beta=90°$) the boundary planes.

In both cases, we have observed layer-by-layer growth across the entire surface and not only above the crystalline regions. However, we find that the grains induce a loss of crystallinity, particularly for an incident angle parallel to the interface ($\beta=0°$). The lateral extent of these amorphous regions increases during deposition at the expense of the crystalline areas.

VI. CONCLUSION

We have developed an embedded-atom potential for Ti that models not only bulk systems[13] but also Ti surfaces, clusters, and other low coordinated Ti structures. The new potential reproduces the average bond lengths and binding energies of clusters with up to nine atoms with less than 10% error and accurately predicts diffusion barriers on Ti(0001) surfaces. We have employed this new potential to study atomistically thin-film growth of Ti by physical vapor deposition, focusing on the structure and role of grain boundaries during growth. Systematic insights could be gained by invoking the concept of coincidence-site lattices that allow one to quantitatively characterize the geometry of the experimentally dominant grain boundaries in Ti. We find tilt grain boundaries to influence the surface geometry and binding energy of an adatom only in its immediate vicinity (≈ 5 Å) and have no long-range effects, The energy barrier for adatom diffusion across the grain boundary ($\Delta E_{GB}=1.21$ eV) is much higher than the minimal diffusion barrier on the perfect crystalline (0001) plane ($\Delta E_{(0001)}=0.38$ eV). Thus, a grain boundary forms a massive barrier for surface diffusion. In addition, we find small isolated grains to decay by thermal motion at temperatures above 150 K. At room temperature, only grains with a diameter larger than 33 Å remain stable. The deposition of atoms on grain boundaries shows layer-by-layer growth, but the appearance of amorphous regions that spread rapidly with deposition time around the grain boundaries.

*Electronic address: hammerschmidt@fhi-berlin.mpg.de

[1] D. C. Rapaport, *The Art of Molecular Dynamics Simulation* (Cambridge University Press, Cambridge, 1995).
[2] M. P. Allen and D. J. Tildesley, *Computer Simulation of Liquids* (Oxford University Press, Oxford, 1996).
[3] D. Frenkel, and B. Smit, *Understanding Molecular Simulation* (Academic Press, San Diego, 1996).
[4] G. H. Gilmer, H. Huang, T. D. de la Rubia, J. Dalla Torre, and F. Baumann, Thin Solid Films **365**, 189 (2000).
[5] M. S. Daw and M. I. Baskes, Phys. Rev. B **29**, 6443 (1984).
[6] M. S. Daw, Phys. Rev. B **39**, 7441 (1988).
[7] M. S. Daw, S. M. Foiles, and M. I. Baskes, Mater. Sci. Rep. **9**, 251 (1993).
[8] F. H. Baumann, D. L. Chopp, T. D. de la Rubia, G. H. Gilmer, J. E. Greene, H. Huang, S. Kodambaka, P. O'Sullivan, and I. Petrov, Mater. Res. Bull. **26**, 182 (2001).

[9] J. A. Thornton, Annu. Rev. Mater. Sci. **7**, 239 (1977).
[10] C. R. M. Grovenor, H. T. G. Hentzell, and D. A. Smith, Acta Metall. **32**, 773 (1984).
[11] R. I. Hedge, R. W. Fiordalice, and D. Kolar, J. Electrochem. Soc. **144**, 1849 (1997).
[12] E. F. Chinaglia and I. C. Oppenheim, in *Mechanisms of Surface and Microstructure Evolution in Deposited Films and Film Structures*, edited by J. Sanchez *et al.*, MRS Symp. Proc. No. 672 (Materials Research Society, Warrendale, 2001), p. O3.26.1.
[13] G. J. Ackland, Philos. Mag. A **66**, 917 (1992).
[14] U. Hansen and A. Kersch, Phys. Rev. B **60**, 14417 (1999).
[15] F. Much, M. Ahr, M. Biehl, and W. Kinzel, Comput. Phys. Commun. **147**, 226 (2002).
[16] G. Henkelman and H. Jonsson, J. Chem. Phys. **115**, 9657 (2001).
[17] A. Kersch (private communication).
[18] T. Hara, T. Nomura, R. C. Mosley, H. Suzuki, and K. Sone, J. Vac. Sci. Technol. A **12**, 506 (1993).
[19] I. Kaur, Y. Mishin, and W. Gust, *Fundamentals of Grain and Interphase Boundary Diffusion* (Wiley, New York, 1995).
[20] A. H. King and F.-R. Chen, J. Phys. C **10**, 195 (1988).
[21] J. G. Antonopoulos, P. Delavignette, T. Karakostas, P. Komniou, E. Laurent-Pinson, S. Lay, G. Nouet, and J. Vicens, Colloq. Phys. **C1**, 61 (1990).
[22] J. H. Li, Q. Kang, X. G. Ning, C. B. Zhang, K. L. Wu, J. Gong, and H. Q. Ye, Scr. Metall. Mater. **29**, 1621 (1993).
[23] M. A. Fortes, Phys. Status Solidi B **54**, 311 (1972).
[24] G. A. Bruggeman, G. H. Bishop, and W. H. Hartt, in *The Nature And Behaviour Of Grain Boundaries*, edited by H. Hu (AIME, Littleton, CO, 1972).
[25] I. Mac Laren and M. Aindow, Philos. Mag. Lett. **73**, 217 (1996).
[26] S. Wang and M. Aindow, Mater. Sci. Forum **294–296**, 309 (1999).
[27] Y. C. Wang, D. X. Li, and H. Q. Ye, Philos. Mag. A **73**, 213 (1996).
[28] Y. C. Wang, D. X. Li, and H. Q. Ye, Scr. Mater. **34**, 735 (1999).
[29] I. Mac Laren and M. Aindow, Philos. Mag. A **76**, 871 (1997).
[30] M. Doverstal, B. Lindgren, U. Sassenberg, C. A. Arrington, and M. D. Morse, J. Chem. Phys. **97**, 7087 (1992).
[31] S. H. Wei, Z. Zeng, J. Q. You, X. H. Yan, and X. G. Gong, J. Chem. Phys. **113**, 11 127 (2000).
[32] J. Zhao, Q. Qiu, B. Wang, J. Wang, and G. Wang, Solid State Commun. **118**, 157 (2001).
[33] L. M. Russon, S. A. Heldecke, M. K. Birke, J. Conceicao, M. D. Morse, and P. B. Armentrout, J. Chem. Phys. **100**, 4747 (1994).
[34] C. W. Bauschlicher, H. Partridge, S. R. Langhoff, and M. Rosi, J. Chem. Phys. **95**, 1057 (1991).
[35] H. D. Shih, F. Jona, D. W. Jepsen, and P. M. Marcus, J. Phys. C **9**, 1405 (1976).
[36] P. J. Feibelman, Phys. Rev. B **53**, 13 740 (1996).
[37] P. J. Feibelman, Surf. Sci. **360**, 297 (1996).
[38] G. Teeter and J. L. Erskine, Phys. Rev. B **61**, 13 929 (2000).
[39] Z. Szczudlo, A. Ciszewski, and Y. B. Losovyj, Appl. Surf. Sci. **174**, 138 (2001).
[40] G. G. Vladimirov, B. K. Medvedev, and I. L. Sokol'skaya, Sov. Phys. Solid State **12**, 1118 (1970).
[41] J. R. Anderson and N. Thompson, Surf. Sci. **26**, 397 (1971).
[42] M.-C. Wu, J. S. Corneille, and D. W. Goodman, Surf. Sci. **255**, L536 (1991).
[43] G. L. Kellogg, Surf. Sci. Rep. **21**, 1 (1994).
[44] T. Biernat and A. M. Dabrowski, Vacuum **63**, 113 (2001).
[45] W. C. Liu, C. H. Woo, and H. Huang, J. Comput.-Aided Mater. Des. **6**, 311 (1999).
[46] L. E. Murr, *Interfacial Phenomena in Metals and Alloys* (Addison-Wesley, New York, 1975), p. 101.
[47] P. G. Partridge, Metall. Rev. **12**, 169 (1967).
[48] P. B. Legrand, Philos. Mag. B **49**, 271 (1985).
[49] P. B. Legrand, Philos. Mag. A **52**, 83 (1985).
[50] A. Girshick, A. M. Bratkovsky, D. G. Pettifor, and V. Vitek, Philos. Mag. A **77**, 981 (1998).
[51] A. Girshick, D. G. Pettifor, and V. Vitek, Philos. Mag. A **77**, 999 (1998).
[52] A. Kersch and U. Hansen, J. Vac. Sci. Technol. A **20**, 1284 (2002).
[53] Y. C. Wang and H. Q. Ye, Philos. Mag. A **75**, 261 (1997).
[54] H. J. C. Berendsen, J. P. M. Postma, W. F. van Gunsteren, A. DiNola, and J. R. Haak, J. Chem. Phys. **81**, 3684 (1984).